arXiv:1511.03035v1 [cond-mat.mes-hall] 10 Nov 2015

Direct Observation of Propagating Gigahertz Coherent Guided Acoustic Phonons in Free Standing Single Copper Nanowires

Cyril Jean,[†,‡] Laurent Belliard,[*,†,‡] Thomas W. Cornelius,[¶] Olivier Thomas,[¶] Maria Eugenia Toimil-Molares,[§] Marco Cassinelli,[§] Loïc Becerra,[†,‡] and Bernard Perrin[†,‡]

Sorbonne Universités, UPMC Univ Paris 06, UMR 7588, Institut des NanoSciences de Paris, F-75005, Paris, France , CNRS, UMR 7588, Institut des NanoSciences de Paris, F-75005, Paris, France , Aix-Marseille Université, CNRS UMR 7334, IM2NP, F-13397 Marseille Cedex, France , and GSI Helmholtz Centre for Heavy Ion Research, D-64291 Darmstadt, Germany

E-mail: Laurent.Belliard@upmc.fr

[*]To whom correspondence should be addressed

[†]Sorbonne Universités, UPMC Univ Paris 06, UMR 7588, Institut des NanoSciences de Paris, F-75005, Paris, France

[‡]CNRS, UMR 7588, Institut des NanoSciences de Paris, F-75005, Paris, France

[¶]Aix-Marseille Université, CNRS UMR 7334, IM2NP, F-13397 Marseille Cedex, France

[§]GSI Helmholtz Centre for Heavy Ion Research, D-64291 Darmstadt, Germany

Abstract

We report on gigahertz acoustic phonon waveguiding in free standing single copper nanowires studied by femtosecond transient reflectivity measurements. The results are discussed on the basis of the semi-analytical resolution of the Pochhammer and Chree equation. The spreading of the generated Gaussian wave packet of two different modes is derived analytically and compared with the observed oscillations of the sample reflectivity. These experiments provide a unique way to independently obtain geometrical and material characterization. This direct observation of coherent guided acoustic phonons in a single nano-objet is also the first step towards nanolateral size acoustic transducer and comprehensive studies of the thermal properties of nanowires.

During the last decade, nanoscale confinement has stimulated wide fundamental and technological interests in various fields such as photonics,[1] electronics,[2] chemistry[3] or biology.[4,5] The impact of size reduction down to the nanoscale on acoustic response also attracts considerable attention.[6] Fundamental motivations include testing the validity of the classical continuum theory of elasticity at the nanoscale.[7,8] A better understanding of the phonon behavior in nanostructures is also crucial to design MEMS nanoresonators.[9] Confinement deeply modifies the acoustic dispersion relations compared with the bulk counterpart. Such modifications strongly influences the thermal[10,11] and electronic[12] properties of the nanostructures. Time resolved optical spectroscopy is now considered a powerful tool to address phonon properties in single nanoparticles. In such an approach, thermal expansion induced by fast lattice heating created by femtosecond laser absorption, is optically detected in transmission or reflection geometry in far or near field.[13–15] Since the pioneer work of van Dijk *et al.*,[16] which investigated the dynamic response of single gold nanospheres, a large variety of materials and particle shapes have been investigated including nanostructures,[17–19] nanowires,[20–22] nanorings,[23] nanocubes,[24] nanorods[25,26] or dimer nanoparticules.[27] These investigations revealed that the system's vibration eigenmodes are strongly correlated with different parameters like size, shape, material and coupling with the surroundings. Recently, to circumvent the drawback linked to the breathing mode's huge damping rate, which

occurs due to the interaction between the nanostructure and the substrate, free standing nanowires have been investigated.[21] The main advantage of this geometry lies in the obtention of resonators with high quality factors, thus allowing a better understanding of their elastic properties.[28,29] In parallel guided acoustic phonons inside nanowires emerge as promising candidates for nanoacoustic wave generation with nanoscale spotsize, which could prove useful to design nanodevices for three-dimensional noninvasive ultrasonic imaging[30] with nanometer resolutions. Confined[31] and propagating[32] acoustic waves have been reported recently in a single microfiber (with diameter > 30 μm). However, up to now guided phonons modes propagation in nanowires has been adressed only for a bundle of 75 nm GaN nanowires[33] and consequently the results were very sensitive to the inhomogeneous broadening of the acoustic features due to averaging on nanowires of different dimensions.

In this letter we provide evidence of the propagation of gigahertz coherent guided acoustic phonons in single free standing nanowires. Beyond the intrinsic novelty of this direct experimental observation on a single nano-object, the generation and detection of nanoacoustic waves emerge as a useful characterization tool. We first show that the experimental investigation of confined modes only allows the determination of the characteristic sound velocities v_L and v_T[1], the radius a of the wire has to be determined by an other characterization method such as Scanning Electron Microscopy (SEM). We then analyze the generation and propagation of coherent guided phonons in single copper nanowires. We are able to follow two phonon modes along the nanowire axis. We first observe the propagation of a gaussian wave packet corresponding to the propagation of a pure radial breathing mode of frequency around 15.6 GHz which exhibits a parabolic dispersion curve. A pulse, characteristic of an expansionnal mode associated with a linear dispersion curve is also observed. The observed oscillations of the sample reflectivity are compared to the predicted behavior in an infinite cylinder.

Since the last decade, many works have been devoted to time resolved spectroscopy on supported nanowires. More recently, free standing geometries have demonstrated a better acoustic

[1] $v_L = \sqrt{E(1-\nu)/(\rho(1+\nu)(1-2\nu))}$ is the longitudinal sound velocity, : $v_T = \sqrt{E/(2\rho(1+\nu))}$ is the transverse sound velocity. E, ν and ρ are the Young modulus, the Poisson ratio and the density of the material respectively.

confinement. Our polycrystalline copper nanowires are prepared by electrodeposition in etched ion-track membranes as described elsewhere.[28,34] In order to reduce the energy dissipation through the silicon substrate, the wires are dispersed on a silicon wafer structured with periodic trenches (Fig. 1) fabricated by lithography and anisotropic silicon etching.[28] Ultrafast pump-probe spectroscopy experiments are performed using a mode-locked Ti:sapphire (MAI-TAI Spectra) laser source operating at 800 nm with a pulse duration of 100 fs at a repetition rate of 78.8 MHz. The pump beam is modulated at 1.8 MHz to perform synchronous detection on the sample reflectivity. Both pump and probe beams are focused by an objective with a $NA = 0.9$ and are normally incident on the sample. The probe beam is fixed on a XY piezoelectric stage such as it is laterally positionned with respect to the pump beam. To avoid scattered light coming from the pump beam, a two-color expriment is performed by doubling the pump frequency ($\lambda = 400$ nm) with a nonlinear cystal. A dichroic filter located in front of the diode system suppresses the light of the pump beam, its power is reduced around 300 μW and the power of the probe beam does not exceed 30 μW. With such experimental conditions, we stay in the thermoelastic regime, the acoustic signal and the optical reflectivity remain stable during all the average processing. The reflectivity from the sample is measured by an avalanche photodiode and analyzed with a lock-in amplifier. A maximum pump-probe time delay equal to 12 ns is achieved using a mobile reflector system mounted on a translation stage.

We investigate nanowires, whose diameter D is around 200 nm and whose total length L exceeds 5 μm, in the frame of the elasticity theory of waves developped by Pochhammer[35] and Chree.[36] Our cylinders are considered as infinite given their large aspect ratio $L/D > 25$. Due to diffraction limitation, the pump laser spot size is larger than the nanowires diameter, leading to homogeneous dilatation. We thus consider no azimutal dependance of the modes in the following. Zero radial stress at the surface is the boundary condition for a free standing cylinder. Applying these conditions yields the following dispersion equation[37]

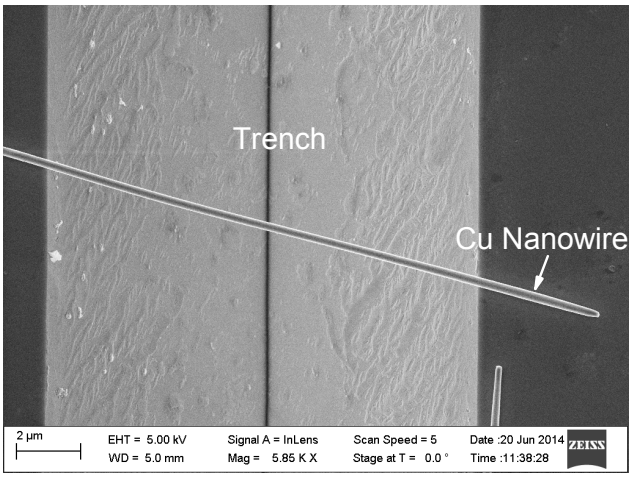

Figure 1: Scanning electron microscope image of a 200 nm diameter copper nanowire placed across pyramidal trenches fabricated by lithography and anisotropic silicon etching.

$$2P_n\left(Q_n^2+K^2\right)\mathrm{J}_1(P_n)\mathrm{J}_1(Q_n)-\left(Q_n^2-K^2\right)^2\mathrm{J}_0(P_n)\mathrm{J}_1(Q_n) \\ -4K^2P_nQ_n\mathrm{J}_1(P_n)\mathrm{J}_0(Q_n)=0 \tag{1}$$

where J_0 and J_1 are respectively the spherical Bessel function of the first kind of order zero and one. The natural number n is the order of the longitudinal axially symmetric mode, $\mathrm{L}(0,\mathrm{n})$, according to Silk and Bainton naming convention.[39] $P_n^2=(X_n/\beta)^2-K^2$ and $Q_n^2=X_n^2-K^2$. X_n is the reduced pulsation $X_n=\omega_n a/v_T$, $K=ka$ is the reduced wave number and β is a material parameter which exclusively depends of the Poisson ratio ν of the material : $\beta^2=(v_L/v_T)^2=(2-2\nu)/(1-2\nu)$. The dispersion curves of the first nine dilatational modes of a 200 nm diameter copper nanowire with a circular cross section are calculated numerically and reproduced in Fig.2b. At infinite wavelength ($K=0$), equation (1) can be simplified as

$$\mathrm{J}_1\left(\frac{\omega_n a}{v_T}\right)\left[2\frac{v_T}{v_L}\mathrm{J}_1\left(\frac{\omega_n a}{v_L}\right)-\frac{\omega_n a}{v_T}\mathrm{J}_0\left(\frac{\omega_n a}{v_L}\right)\right]=0 \tag{2}$$

It can be shown that the roots of J_1 define modes with a purely axial displacement field. The

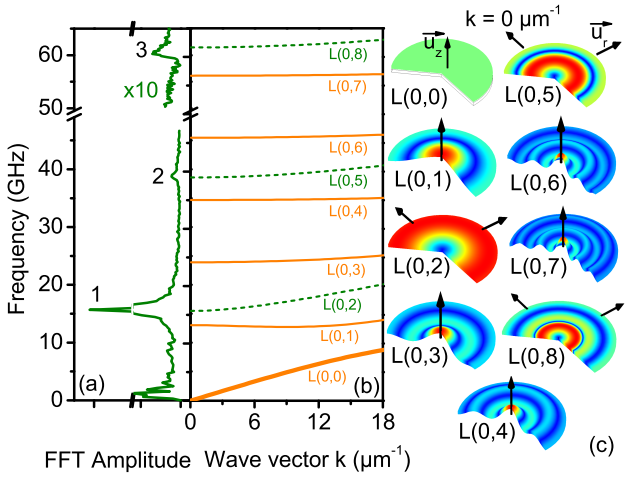

Figure 2: (Color online) (a) : FFT of an experimental oscillatory signal on an autosuspended 200 nm diameter copper nanowire. One can observe the first three breathing modes. (b) : numerically calculated dispersion relation of the nine first longitudinal modes of a 200 nm diameter copper nanowire. (c) : Mode shapes of the first eigth non trivial longitudinal eigenmodes calculated at infinite wavelength ($K = 0$) using 2D axisymmetric finite elements method (FEM). The Young modulus, Poisson ratio and density have been set at 110 GPa, 0.35 and 8700 $\mathrm{kg \cdot m^{-3}}$ respectively, in agreement with usual values for polycrystalline copper.[38] The modes $\mathrm{L}(0,2)$, $\mathrm{L}(0,5)$ and $\mathrm{L}(0,8)$ exhibit purely radial displacement whereas the displacement field of the other six modes is purely axial. Colors represent the magnitude of the displacement : a deep blue color corresponds to a nodal area of the mode shape when the red color means maximum magnitude. Black arrows indicate the displacement field direction.

roots of the second factor $g_n(a, v_L, v_T) = 2v_T/v_L \mathrm{J}_1(\omega_n a/v_L) - \omega_n a/v_T \mathrm{J}_0(\omega_n a/v_L) = 0$ define the well-known breathing modes with a purely radial displacement field. The displacement field distributions of some of these modes are depicted in Fig.2c.

The frequency signature obtained on a single free standing 200 nm diameter copper nanowire with pump and probe superimposed is depicted in Fig.2a. In an infinite wire, excitation and detection mechanisms essentially favor modes exhibiting large radial displacements.[21] Taking advantage of the huge acoustic confinement, the signal exhibits a complex structure composed of the fundamental breathing mode around 15.6 GHz, and its two first harmonics located at 39.6 GHz and 60 GHz. Using this rich vibrational behavior, one can then expect to determine the three nanowire properties (a, v_L, v_T) by solving this non linear inverse problem. However, it doesn't matter how many breathing mode frequencies are experimentally determined since the g_n are homogeneous function of order zero : $g_n(\lambda a, \lambda v_L, \lambda v_T) = g_n(a, v_L, v_T)$ with $\lambda \neq 0$. When a solution is found, there is no unicity. One has to determine the dilatation factor λ with an other set of measurements. For instance, a can be determined using SEM or Atomic Force Microscopy. Our SEM measurements give us a 200 nm nanowire diameter which allows an estimation of the velocity, equal to $v_L = 4.5 \cdot 10^3$ m$\cdot$s^{-1} and $v_T = 2.2 \cdot 10^3$ m$\cdot$s^{-1} for longitudinal and transverse waves respectively, in good adequation with the copper elastic constants.[38] However, finding a single nano-object previously studied by femtosecond transient reflectometry under SEM often results in a very tedious and unfruitful task. Consequently, a means to characterize the material and geometrical properties of nanowires completely with picosecond acoustic measurement remains to be found.

In the following, we show that the determination of the three nanowire properties (a, v_L, v_T) can be adressed by the experimental observation of propagating acoustic nanowaves corresponding to the L$(0,0)$ and L$(0,2)$ modes. It can be demonstrated that, in the case of L$(0,0)$, the first order development of the dispersion relation around $k = 0$ is $\omega = vk$ with $v = \sqrt{E/\rho}$. We also demonstrated that the development of the dispersion equation around $K = 0$ of the first radial breathing mode L$(0,2)$ that verifies $2v_L/v_T \mathrm{J}_1(\omega_2 a/v_L) - \omega_2 a/v_T \mathrm{J}_0(\omega_2 a/v_L) = 0$ is parabolic : $\omega a/v_L = \omega_2 a/v_L + \delta(ka)^2$ with

$$\delta = \frac{4\left(2p_2\beta \mathrm{J}_0(p_2\beta) - 3\mathrm{J}_1(p_2\beta)\right) + p_2^2\beta^4 \mathrm{J}_1(p_2\beta)}{2p_2 \mathrm{J}_1(p_2\beta)\left(p_2^2\beta^4 + 4(1-\beta^2)\right)} \tag{3}$$

where $p_2 = P_2(K=0) = \omega_2 a/v_L$. The time and space evolution of a wave packet resulting from a propagation with linear and parabolic dispersion relation is calculated, and the general form $\omega(k) = \alpha k^2 + \beta k + \gamma$ is chosen. Assuming a gaussian pump beam with diameter $\sigma = 0.5$ μm at $1/e^2$ and a uniform radial dilation of the nanowire at $z = 0$ and $t = 0$, the initial deformation is $\eta(z) = 4/(\sigma\sqrt{2\pi})\exp\left(-8z^2/\sigma^2\right)$. As we do not provide physical insight on the excitation mechanism, we suppose no mode dependence in the excitation amplitude. According to this zero order approximation, each k mode is excited with the same unitary amplitude, leading to $\hat{\eta}(k) = \int_{-\infty}^{\infty} \eta(z)\exp(\mathrm{i}kz)\,\mathrm{d}z = \exp\left(-k^2\sigma^2/32\right)$. We notice that only wave numbers verifying $k^2\sigma^2/32 < 2$, that is to say $k < 20$ $\mu\mathrm{m}^{-1}$, are excited with significant amplitude. Such a low k amplitude should lead to a small k dependance in the excitation amplitude of each mode which justifies the above approximation. Each k mode propagates as a plane-wave $\exp(\mathrm{i}(kz - \omega(k)t))$ along the z axis of the wire resulting in the following gaussian wave packet

$$\begin{aligned} \psi(z,t) &= \int_{-\infty}^{\infty} \hat{\eta}(k)\exp(\mathrm{i}(kz - \omega(k)t))\,\mathrm{d}k & (4) \\ &= \frac{\sqrt{32\pi}}{\sqrt{\sigma^2 + 32i\alpha t}} \exp\left(-\frac{8(\beta t - z)^2}{\sigma^2 + 32\mathrm{i}\alpha t}\right)\exp(-\mathrm{i}\gamma t) & (5) \end{aligned}$$

As the detection is achieved at $z = z_0$ using a gaussian probe beam, with diameter $\nu = 1$ μm at $1/e^2$, a convolution with $\phi(z) = 4/(\nu\sqrt{2\pi})\exp\left(-8(z-z_0)^2/\nu^2\right)$ is applied. Finally, the experimental signal at a distance z_0 from the pump beam may be assumed to be proportional to the real part of the following equation

$$\Delta r(t) = \int_{-\infty}^{\infty} \phi(z)\psi(z,t)\mathrm{d}z \tag{6}$$

$$= \frac{\sqrt{32\pi}\exp(-\mathrm{i}\gamma t)}{\sqrt{\nu^2+\sigma^2+32\mathrm{i}\alpha t}} \exp\left(-\frac{8(z_0-\beta t)^2}{\nu^2+\sigma^2+32\mathrm{i}\alpha t}\right) \tag{7}$$

We can also extract the envelop of the gaussian wave packet with the modulus of $\Delta r(t)$. In the following, we will discuss the experimental results in the light of this analytical expression. Considering the L$(0,0)$ mode, we will take $\alpha = 0$, $\beta = \sqrt{E/\rho}$, $\gamma = \omega_0 = 0$. Considering the L$(0,2)$ mode, the parameter values will be $\alpha = \delta v_L a$, $\beta = 0$, $\gamma = \omega_2$.

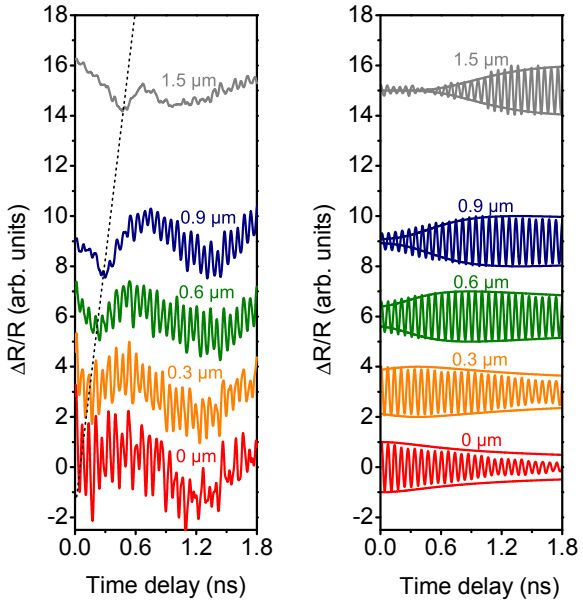

Figure 3: (Color online) Left (a) : Raw data of the transient reflectivity obtained on a single free standing 200 nm diameter copper nanowire. The distance labeled above each curve is the pump-probe separation z_0. The high-frequency signal is the 15.6 GHz first radial breathing mode. The additional feature that appears at 600 nm with a probe delay of 170 ps and at 1500 nm with a probe delay of 400 ps is the signature of the L$(0,0)$ mode : the black dotted line follows the maximum of the deformation and demonstrates a linear propagation. Right (b) : Same signal normalized to $[-1,1]$ with a second order band-pass filter centered at the first radial breathing mode frequency of 15.6 GHz. We thus highlight the dispersion of the first breathing mode. The solid line envelop is $|\Delta r(t)|$ calculated analytically with $\alpha = 1.7 \cdot 10^{-4}$ m$^2 \cdot$s^{-1}, $\beta = 0$, $\gamma = 15.6$ GHz, $\nu = 1$ μm and $\sigma = 0.5$ μm. A comparison between non-filtered Fig. 3a and filtered Fig. 3b shows that there is no artifact added by such filtering process.âĂİ

In order to be sensitive to the propagation phenomenon, the pump and probe beams have to be separated using an experimental setup which allows to tilt the probe before the last objective lens.[23] The transient reflectivity obtained on a single free standing 200 nm diameter copper nanowire, with pump-probe separation ranging from $z_0 = 0$ nm to $z_0 = 1.5$ μm, is presented in Fig. 3. The distance labeled above each curve is the pump-probe separation z_0. At small pump-probe separation, the signal is mainly composed of a high-frequency signature at 15.6 GHz which corresponds to the first radial breathing mode. As the pump-probe separation increases, this high-frequency wave-packet shifts to a longer time delay as expected for a propagation guided along the nanowire axis. However, this signal suffers strong attenuation which results in a poor signal-to-noise ratio at large pump-probe separations. To get rid of the attenuation and to increase the signal-to-noise ratio at large pump-probe separation, the signal is normalized to $[-1,1]$ and a band-pass filter centered at 15.6 GHz is applied. The resulting signal is ploted in Fig. 3b. The strong dispersion of this mode is clearly revealed. The solid line envelop $|\Delta r(t)|$ calculated analytically with a purely parabolic dispersion relation : $\alpha = 1.7 \cdot 10^{-4}$ m$^2 \cdot$s^{-1}, $\beta = 0$, $\gamma = 15.6$ GHz, $\nu = 1$ μm and $\sigma = 0.5$ μm, fits very well with the whole set of experimental results. It is remarkable that the extracted value α is the numerical result of $\delta v_L a$ with $v_L = 4.5 \cdot 10^3$ m$\cdot$s^{-1}, $v_T = 2.2 \cdot 10^3$ m$\cdot$s^{-1} and $a = 100$ nm, which are the values obtained experimentally using the breathing mode at $K = 0$ and the SEM measurements. Furthermore, a close inspection of figure 3 reveals that a signal deformation appears at $z_0 = 600$ nm with a probe delay of 170 ps and propagates through $z_0 = 1500$ nm with a probe delay of 400 ps. This signature can be associated to the $\mathrm{L}(0,0)$ mode. It is interesting to note that the displacement field distribution of mode $\mathrm{L}(0,0)$ at an infinite wavelength calculated with three dimensional FEM presents no radial displacement explaining its absence when the pump and probe are superimposed. On the contrary, the displacement field distribution of mode $\mathrm{L}(0,0)$ at $k \approx 20$ μm^{-1} calculated with three dimensional FEM shows a significant radial displacement. Therefore, this mode will be more easily detected with small pump and probe beams which provide a large wave vector distribution. We are then able to detect this $\mathrm{L}(0,0)$ mode when the pump-probe spatial separation inscreases. To further investigate this signal, we explore larger pump-probe

spatial separation as reported in Fig. 4.

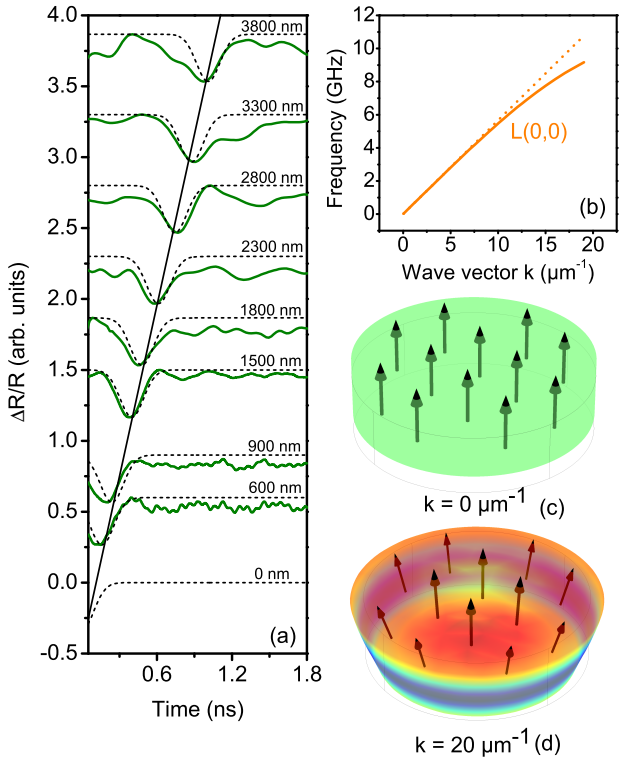

Figure 4: (Color online) (a) : Transient reflectivity signal obtained on a single free standing 200 nm diameter copper nanowire with a 200 ms time integration constant that acts as a hardware low-pass filter. Signals are normalized to $[-0.3,0]$. The distance label above each curve corresponds to the pump-probe separation z_0. The dotted line is $|\Delta r(t)|$ calculated analytically with $\alpha = 0$, $\beta = 3.6 \cdot 10^3$ m$\cdot$s^{-1}, $\gamma = 0$, $\nu = 1$ μm and $\sigma = 0.5$ μm. The black solid line follows the maximum of the deformation and demonstrates a linear propagation (b) : Dispersion relation of the L$(0,0)$ branch. The solid line corresponds to the exact relation, the dotted line is the linear approximation $\omega = \sqrt{E/\rho}k$. (c) : The displacement field distribution of mode L$(0,0)$ at infinite wavelength calculated with three dimensional FEM exhibits no radial displacement. (d) : The displacement field distribution of mode L$(0,0)$ at $k \approx 20$ μm^{-1} calculated with three dimensional FEM shows a significant radial displacement.

This transient reflectivity signal is obtained on a single free standing 200 nm diameter copper nanowire with a 200 ms time integration constant that acts as a low-pass filter and increases the signal-to-noise ratio dramatically, which is much needed at distances as large as 3.8 μm. Signals are normalized to $[-0.3,0]$ to get rid of the attenuation which is not taken into acount in our theorical model. The distance label above each curve corresponds to the pump-probe separation z_0. The dotted line is $|\Delta r(t)|$ calculated analytically with $\alpha = 0$, $\beta = 3.6 \cdot 10^3$ m$\cdot$s^{-1}, $\gamma = 0$,

$\nu = 1$ μm and $\sigma = 0.5$ μm. Such a best fit value is consistant with $\sqrt{E/\rho}$. Unlike the complex expression of the parabolic coefficient δ of the L$(0,2)$ mode and the resulting complex spreading of the gaussian wave-packet in Fig. 3, this L$(0,0)$ mode provides a unique way to get the Young modulus of a material independently of any geometrical dimensions. Simple and precise reading of the deformation maximum's propagation velocity gives direct access to the Young modulus. Finally, measuring $v = 3.6 \cdot 10^3$ m$\cdot$s^{-1}, $f_2 = 15.6$ GHz and $f_5 = 39.6$ GHz gives : $a = 91 \pm 3$ nm, $v_L = 4.1 \pm 0.2 \cdot 10^3$ m$\cdot$s^{-1} and $v_T = 2.2 \pm 0.1 \cdot 10^3$ m$\cdot$s^{-1}. These values are in good agreement both with copper elastic constants and SEM measurements.

In summary, we have investigated the propagation of two guided modes in single free standing copper nanowires. By considerably reducing the relaxation channel towards the substrate, the suspended nanowires provide a unique tool to observe the propagation of gigahertz coherent acoustic waves with spatial separations between generation and detection as large as 4 μm. A rigorous approach allows us to assign the main components of the reflectometry signal to a precise acoustic mode. These experimental observations also lead to two equations that accurately complete the set of equations at infinite wavelength thus allowing the determination of elastic properties as well as the geometrical radius a of the nanowire. Beyond this new way to achieve material and geometrical characterization through picosecond acoustic experiment, this study paves the way to use nanowires as nanometric lateral size acoustic transducers.

References

(1) Maier, S. A.; Brongersma, M. L.; Kik, P. G.; Meltzer, S.; Requicha, A. A. G.; Atwater, H. A. Plasmonics – A Route to Nanoscale Optical Devices. *Adv. Mat.* **2001**, *13*, 1501–1505.

(2) Chang, D. E.; Sørensen, A. S.; Demler, E. A.; Lukin, M. D. A Single-Photon Transistor Using Nanoscale Surface Plasmons. *Nat. Phys.* **2007**, *3*, 807–812.

(3) Novo, C.; Funston, A. M.; Mulvaney, P. Direct Observation of Chemical Reactions on Single Gold Nanocrystals Using Surface Plasmon Spectroscopy. *Nat. Nano.* **2008**, *3*, 598–602.

(4) Huang, X.; El-Sayed, I. H.; Qian, W.; El-Sayed, M. A. Cancer Cell Imaging and Photothermal Therapy in the Near-Infrared Region by Using Gold Nanorods. *J. Am. Chem. Soc.* **2006**, *128*, 2115–2120.

(5) Hirsch, L. R.; Stafford, R. J.; Bankson, J. a.; Sershen, S. R.; Rivera, B.; Price, R. E.; Hazle, J. D.; Halas, N. J.; West, J. L. Nanoshell-Mediated Near-Infrared Thermal Therapy of Tumors under Magnetic Resonance Guidance. *P. Natl. Acad. Sci. USA* **2003**, *100*, 13549–54.

(6) Major, T. A.; Lo, S. S.; Yu, K.; Hartland, G. V. Time-Resolved Studies of the Acoustic Vibrational Modes of Metal and Semiconductor Nano-objects. *J. Phys. Chem. Lett.* **2014**, *5*, 866–874.

(7) Liang, H.; Upmanyu, M.; Huang, H. Size-Dependent Elasticity of Nanowires: Nonlinear Effects. *Phys. Rev. B* **2005**, *71*, 241403.

(8) Juvé, V.; Crut, A.; Maioli, P.; Pellarin, M.; Broyer, M.; Del Fatti, N.; Vallée, F. Probing Elasticity at theNanoscale: Terahertz Acoustic Vibration of Small Metal Nanoparticles. *Nano Lett.* **2010**, *10*, 1853–8.

(9) Feng, X. L.; He, R.; Yang, P.; Roukes, M. L. Very High Frequency Silicon Nanowire Electromechanical Resonators. *Nano Lett.* **2007**, *7*, 1953–1959.

(10) Mingo, N.; Yang, L.; Li, D.; Majumdar, A. Predicting the Thermal Conductivity of Si and Ge Nanowires. *Nano Lett.* **2003**, *3*, 1713–1716.

(11) Boukai, A. I.; Bunimovich, Y.; Tahir-Kheli, J.; Yu, J.-K.; Goddard, W. A.; Heath, J. R. Silicon Nanowires as Efficient Thermoelectric Materials. *Nature* **2008**, *451*, 168–71.

(12) Bannov, N.; Aristov, V.; Mitin, V.; Stroscio, M. A. Electron relaxation Times Due to the Deformation-PotentialInteraction of Electrons with Confined Acoustic Phonons in a Free-Standing Quantum Well. *Phys. Rev. B* **1995**, *51*, 9930–9942.

(13) Thomsen, C.; Grahn, H. T.; Maris, H. J.; Tauc, J. Surface Generation and Detection of Phonons by Picosecond Light Pulses. *Phys. Rev. B* **1986**, *34*, 4129–4138.

(14) Siry, P.; Belliard, L.; Perrin, B. Picosecond Acoustics with Very High Lateral Resolution. *Acta Acust. United Ac.* **2003**, *89*, 925–929.

(15) Vertikov, A.; Kuball, M.; Nurmikko, A. V.; Maris, H. J. Time-Resolved Pump-Probe Experiments with Subwavelength Lateral Resolution. *Applied Physics Letters* **1996**, *69*, 2465.

(16) van Dijk, M.; Lippitz, M.; Orrit, M. Detection of Acoustic Oscillations of Single Gold Nanospheres by Time-Resolved Interferometry. *Phys. Rev. Lett.* **2005**, *95*, 267406.

(17) Burgin, J.; Langot, P.; Del Fatti, N.; VallÃl'e, F.; Huang, W.; El-Sayed, M. A. Time-Resolved Investigation of the Acoustic Vibration of a Single Gold Nanoprism Pair. *J. Phys. Chem. C* **2008**, *112*, 11231–11235.

(18) Bienville, T.; Robillard, J. F.; Belliard, L.; Roch-Jeune, I.; Devos, A.; Perrin, B. Individual and Collective Vibrational Modes of Nanostructures Studied by Picosecond Ultrasonics. *Ultrasonics* **2006**, *44 Suppl 1*, e1289–94.

(19) Amziane, A.; Belliard, L.; Decremps, F.; Perrin, B. Ultrafast Acoustic Resonance Spectroscopy of Gold Nanostructures: Towards a Generation of Tunable Transverse Waves. *Phys. Rev. B* **2011**, *83*, 014102.

(20) Staleva, H.; Hartland, G. V. Vibrational Dynamics of Silver Nanocubes and Nanowires Studied by Single-Particle Transient Absorption Spectroscopy. *Adv. Funct. Mater.* **2008**, *18*, 3809–3817.

(21) Major, T. A.; Crut, A.; Gao, B.; Lo, S. S.; Del Fatti, N.; Vallée, F.; Hartland, G. V. Damping of the Acoustic Vibrations of a Suspended Gold Nanowire in Air and Water Environments. *Phys. Chem. Chem. Phys.* **2013**, *15*, 4169–76.

(22) Staleva, H.; Skrabalak, S. E.; Carey, C. R.; Kosel, T.; Xia, Y.; Hartland, G. V. Coupling to Light, and Transport and Dissipation of Energy in Silver Nanowires. *Phys. Chem. Chem. Phys.* **2009**, *11*, 5889–5896.

(23) Kelf, T. A.; Tanaka, Y.; Matsuda, O.; Larsson, E. M.; Sutherland, D. S.; Wright, O. B. Ultrafast Vibrations of Gold Nanorings. *Nano Lett.* **2011**, *11*, 3893–3898.

(24) Staleva, H.; Hartland, G. V. Transient Absorption Studies of Single Silver Nanocubes. *J. Phys. Chem. C* **2008**, *112*, 7535–7539.

(25) Cardinal, M. F.; Mongin, D.; Crut, A.; Maioli, P.; RodrÃ■guez-GonzÃąlez, B.; PÃl'rez-Juste, J.; Liz-MarzÃąn, L. M.; Del Fatti, N.; VallÃl'e, F. Acoustic Vibrations in Bimetallic Au@Pd Core-Shell Nanorods. *J. Phys. Chem. Lett.* **2012**, *3*, 613–619.

(26) Zijlstra, P.; Tchebotareva, A. L.; Chon, J. W.; Gu, M.; Orrit, M. Acoustic Oscillations and Elastic Moduli of Single Gold Nanorods. *Nano Lett.* **2008**, *8*, 3493–3497.

(27) Jais, P. M.; Murray, D. B.; Merlin, R.; Bragas, A. V. Metal Nanoparticle Ensembles: Tunable Laser Pulses Distinguish Monomer from Dimer Vibrations. *Nano Lett.* **2011**, *11*, 3685–3689.

(28) Belliard, L.; Cornelius, T. W.; Perrin, B.; Kacemi, N.; Becerra, L.; Thomas, O.; Eugenia Toimil-Molares, M.; Cassinelli, M. Vibrational Response of Free Standing Single Copper Nanowire Through Transient Reflectivity Microscopy. *J. Appl. Phys.* **2013**, *114*, 193509.

(29) Ristow, O.; Merklein, M.; Grossmann, M.; Hettich, M.; Schubert, M.; Bruchhausen, A.; Grebing, J.; Erbe, A.; Mounier, D.; Gusev, V. et al. Ultrafast spectroscopy of super high frequency mechanical modes of doubly clamped beams. *Appl. Phys. Lett.* **2013**, *103*, 233114.

(30) Lin, K.-H.; Yu, C.-T.; Sun, S.-Z.; Chen, H.-P.; Pan, C.-C.; Chyi, J.-I.; Huang, S.-W.; Li, P.-C.; Sun, C.-K. Two-Dimensional Nanoultrasonic Imaging by Using Acoustic Nanowaves. *Appl. Phys. Lett.* **2006**, *89*, 043106.

(31) Mounier, D.; Poilâne, C.; Khelfa, H.; Picart, P. Sub-Gigahertz Laser Resonant Ultrasound Spectroscopy for the Evaluation of Elastic Properties of Micrometric Fibers. *Ultrasonics* **2014**, *54*, 259–67.

(32) Khelfa, H.; Mounier, D.; Poilâne, C.; Picart, P. Détermination Expérimentale des Courbes de Dispersion des Modes Guidés se Propageant le Long d'une Fibre Cylindrique Micrométrique. *14ème Congrès Français d'Acoustique* **2014**, 1225–1231.

(33) Mante, P.-A.; Wu, Y.-C.; Lin, Y.-T.; Ho, C.-Y.; Tu, L.-W.; Sun, C.-K. Gigahertz Coherent Guided Acoustic Phonons in AlN/GaN Nanowire Superlattices. *Nano lett.* **2013**, *13*, 1139–44.

(34) Molares, M. T.; Buschmann, V.; Dobrev, D.; Neumann, R.; Scholz, R.; Schuchert, I. U.; Vetter, J. Single-Crystalline Copper Nanowires Produced by Electrochemical Deposition in Polymeric Ion Track Membranes. *Adv. Mater* **2001**, *13*, 62–65.

(35) Pochhammer, L. Über die Fortpflanzungsgeschwindigkeiten kleiner Schwingungen in einem Unbegrenzten Isotropen Kreiszylinder. *J. Reine Angew. Math.* **1876**, *81*, 324.

(36) Chree, C. The Equations of an Isotropic Elastic Solid in Polar and Cylindrical Coordinates, their Solutions and Applications. *Trans. Cambridge Phil. Soc.* **1889**, *14*, 250.

(37) Royer, D.; Dieulesaint, E. *Elastic Waves in Solids I : Free and Guided Propagation*; Springer-Verlag, New York, 2000.

(38) Ledbetter, H.; Naimon, E. Elastic properties of metals and alloys. II. Copper. *J. Phys. Chem. Ref. Data* **1974**, *3*, 897–935.

(39) Silk, M.; Bainton, K. The propagation in metal tubing of ultrasonic wave modes equivalent to Lamb waves. *Ultrasonics* **1979**, *17*, 11–19.

Graphical TOC Entry